A&A 466, 157–164 (2007)
DOI: 10.1051/0004-6361:20066211

Astronomy & Astrophysics

Spectroscopic and light curve characterization of bulge microlensing events⋆,⋆⋆

M. Soto[1,2], D. Minniti[2], and M. Rejkuba[3]

[1] Leiden Observatory, Leiden University, PO Box 9513, 2300 RA Leiden, The Netherlands
e-mail: soto@strw.leidenuniv.nl
[2] Departamento de Astronomía y Astrofísica, P. Universidad Católica de Chile, Av. Vicuña Mackenna, 4860 Santiago, Chile
e-mail: dante@astro.puc.cl
[3] European Southern Observatory, Karl-Schwartzschild-Strasse 2, 85748 Garching, Germany
e-mail: mrejkuba@eso.org

Received 8 August 2006 / Accepted 7 January 2007

ABSTRACT

Aims. Microlensing events have been observed regularly by surveys such as MACHO, OGLE and MOA. They offer an excellent way to probe the galactic structure, kinematics and stellar content. We have undertaken a follow-up study of 16 galactic microlensing events to determine masses and locations of the sources of these events within the Galaxy.
Methods. Spectroscopy allows us to obtain information about the sources of the events. Low resolution spectra obtained with the Magellan I and II telescopes were analyzed to obtain radial velocities, spectral type and extinction by the method of Kane & Sahu. We also present results for the lens of the event using the microlensing light curve when possible. Light curves have been analyzed with the standard and the parallax models.
Results. We have inferred a configuration inside our galaxy for each event, and therefore a lens mass estimation using a suitable galaxy model. Lens mass determination in some cases shows massive lenses that can be considered black hole candidates. This is the case for the events MACHO-98-BLG-6, and OGLE-00-BUL-43. In our sample only three events do not have enough parallax signal for a successful estimation of the lens mass.

Key words. gravitational lensing – stars: kinematics – Galaxy: structure – Galaxy: stellar content

1. Introduction

Microlensing has been considered for a long time an excellent tool for the discovery of massive compact halo objects (Paczyński 1986). The efforts to complete huge surveys in the galactic center and Magellanic Clouds and the improving of the photometric measurements and software techniques have made possible the discovery of many of them (e.g. Alcock et al. 2000a). Nowadays, hundreds of microlensing events are detected every year by collaborative groups such as OGLE and MOA (e.g. Wózniak et al. 2001). They provide real time alerts of events with particular properties. These results are important in studying the structure in our Galaxy, and other topics such as extrasolar planets. The best example of the importance of microlensing is the recent discovery of the first extrasolar planets by microlensing, OGLE-2003-BLG-235/MOA-2003-BLG-53 (Bond et al. 2004), OGLE-2005-BLG-071 (Udalski et al. 2005), and the latest OGLE-2005-BLG-390Lb (Beaulieu et al. 2006).

The presence of large amounts of dark matter in our galaxy can only be detected by galactic microlensing. Microlensing is thus an important source of information on galactic structure and kinematics. The test measurements of optical depths – the probability of seeing a microlensing event at any given instant – by the MACHO and OGLE collaborations (Popowski 2005; Sumi et al. 2006), have shown a good agreement with theoretical predictions (Wood & Mao 2005) and models that show a barred galactic center (Han & Gould 2003).

Although most microlensing events can be explained by standard modeling (constant velocities for the objects in the event), a few of them can be explained by a parallax model (Alcock et al. 1995). In the parallax model it is possible to obtain some information about the lens. Nevertheless, even in this case the degeneracy of the equations cannot be totally broken, and it is not possible to find the mass of the lens directly. However, the equations give us the possibility to estimate the mass of the lens as a function of distance. Velocity dispersions within the bulge and disk are well known, and these should be similar for bulge or disk events (Han & Gould 1997). Adding the constraint on the velocities of the source from spectroscopy, we can make an approximation of the real event configuration within the galaxy. An analysis for each event provides us three dimensional information about the bulge and disk kinematics (Kane & Sahu 2003, henceforth KN03). This sort of analysis with a large sample can

⋆ Based on observations collected with the Magellan telescopes of the Carnegie Institution of Washington, at Las Campanas Observatory in Chile.
⋆⋆ Electronic spectra is only available in electronic form at the CDS via anonymous ftp to cdsarc.u-strasbg.fr (130.79.128.5) or via
http://cdsweb.u-strasbg.fr/cgi-bin/qcat?J/A+A/466/157

Table 1. Radial velocity and magnitude for standard stars.

Name	$V_{\rm HELIO}$ [km s^{-1}]	V (mag)
HR 3418	+24.5	4.45
HR 6136	+7.3	5.40
HR 7429	–23.9	4.45
HR 7430	–30.8	5.14
HD 64606	+93.4	7.44

deliver important information to disentangle the kinematics of the galactic center, which is currently not well constrained.

This paper is organized as follows. In Sect. 2 we briefly give an explanation of the observations and methods used for the data reduction, followed in Sect. 3 by the analysis of the spectra, including spectral types and radial velocities. Section 4 contains the light curve analysis for the same events using the standard theory of galactic microlensing with two models: the standard and the parallax model. In Sect. 5 we combine the results of Sects. 3 and 4 and determine the lens masses. Our results and conclusions are summarized in Sect. 6.

2. Observations and data reduction

The sample of events was selected among microlensing events with a known strong parallax signature. Some of them have been analyzed already (e.g. M99BLG1 and M98BLG6 by Bennett et al. 2002).

The spectroscopic observations were obtained in two runs. The first run was on May 7 and 8, 2002, when we used the Magellan I Baade telescope at Las Campanas Observatory, located in Chile, with the Boller & Chivens spectrograph. The CCD detector had 2048 × 512 pixels, and the grism with 600 l/mm giving a resolution of 1.6 Å/pixel.

The spectra in the second run were observed with the twin Magellan II Clay telescope at Las Campanas Observatory with the spectrograph LDSS-2 (Low Dispersion Spectrograph Survey) on 10 and 11 May 2005. The CCD detector had 2048 × 2048 pixels and we used a grism with 600 l/mm and a resolution of 2.4 Å/pixel. In each observation, spectrophotometric and radial velocity standard stars were observed for the calibration of the spectra and measurement of their radial velocities (Table 1).

Standard bias correction and flat fielding were applied to the data before the extraction of the one dimensional spectra, which was carried out using the IRAF task *apall*. Wavelength calibration was performed using He-Ar-Ne lamp images, with enough lines in the red and blue sides of the spectrum to develop a suitable dispersion solution. Later, the wavelength calibrated spectra were cut to have the same spectral coverage from 4250 Å to 6780 Å for the whole sample. In addition to the wavelength calibration, a flux calibration was performed in each case using two standards: the star LTT3218 in the first run and LTT4816 in the second run. A complete list of the observed spectra of the microlensing event sources appears in Table 2.

The photometric data were obtained directly from MACHO and OGLE web pages. For more details on the image reduction and photometry process see Wózniak et al. (2001) for OGLE and Alcock et al. (1999) for MACHO. An arbitrary zero point was added to the baseline magnitude for programming reasons. This zero point only raises the baseline magnitude and does not change the parallax parameters which depend on the amplification with respect to the baseline.

Table 2. Coordinates, exposure times and *S/N* for the microlensing event spectra.

Event	RA (J2000.0)	Dec (J2000.0)	Exp. (s)	*S/N*
MACHO-99-BLG-1	18:08:50.0	–30:31:56.0	500	28
MACHO-98-BLG-6	17:57:32.8	–28:42:45.4	1200	16
MACHO-96-BLG-12	18:03:53.2	–27:57:35.7	500	25
OGLE-02-BLG-94	17:58:32.8	–29:23:50.7	120	42
OGLE-02-BLG-91	18:09:50.2	–26:05:42.6	900	31
MACHO-96-BLG-4	18:06:12.0	–28:16:52.8	360	45
OGLE-02-BLG-69	17:48:01.0	–21:16:09.3	420	27
MACHO-98-BLG-14	17:59:08.9	–28:24:54.7	600	17
MACHO-104-C	18:03.34.0	–28:00:19.0	600	58
OGLE-00-BUL-43	18:08:43.0	–32:24:39.5	240	54
OGLE-02-BLG-100	18:06:47.9	–34:51:20.5	600	36
OGLE-02-BLG-61	17:35:56.0	–27:16:01.8	600	26
OGLE-99-BLG-19	17:51:10.8	–33:03:44.1	240	51
sc26_2218	17:47:23.3	–34:59:52.4	600	86
sc33_4505	18:05:46.7	–28:25:32.1	600	17
OGLE-03-BLG-47	18:16:30.6	–28:31:21.2	600	79

3. Analysis of spectra

3.1. Radial velocities

The measurements of radial velocities were made by two procedures in IRAF. First, by *rvidlines* for radial velocities standard stars, and second by *fxcor* for the microlensing events. Several exposures were taken for standard stars each night (Table 1).

The measurement of radial velocities with *fxcor* is based on the cross-correlation by Tonry & Davis (1979); the measured spectrum is compared with the template spectrum, and the maximum in the cross-correlation function gives the Doppler shift of the object spectrum. For a correct determination of radial velocities, several standard stars were used. The error was obtained from a Gaussian fit of the cross-correlation function. A suitable *S/N* ratio has been reached in all the spectra, which is necessary for the cross correlation where the error in the determination of the main peak depends on the spectral quality of the template and the object. Therefore, the best measurements were obtained when the *S/N* was large in both spectra; template and source of the event.

One of the advantages of the cross-correlation is that it uses a large number of lines to determine the radial velocities. Nevertheless, some lines with non-stellar origin have been rejected (for instance the line NaD (5889 Å), which has a clear interstellar origin). In all cases, the selection of the region for the cross-correlation was very careful. Noisy regions with poorly defined lines or where the extraction of the spectrum trace typically were weaker were avoided, such as the ends of the spectra.

3.2. Spectral types

Spectral types were measured in order to constrain the properties of the source stars, mainly their distances.

This procedure was performed using the task *synphot*, and it is basically the same as used by KN03. This consists of a fitting of different spectral types from a library over the measured spectrum. In each case the template spectrum is renormalized according to the observed V magnitude of the measured spectrum.

The slope of the measured spectrum is reproduced by the fit of the extinction-free like parameter (Kane & Sahu 2006) based on the standard galactic extinction (Seaton 1979). The χ^2 between the fit and real spectrum was the selection criterion.

Table 3. Radial velocities, spectral type and extinction.

Event	$V_{\rm HELIO}$	Classification	$E(B-V)$
MACHO-99-BLG-1	64 ± 6	G2V	0.93 ± 0.01
MACHO-98-BLG-6	–39 ± 20	G5IV	0.91 ± 0.02
MACHO-96-BLG-12	237 ± 11	G2III	0.93 ± 0.01
OGLE-02-BLG-94	92 ± 51	M3III	0.71 ± 0.13
OGLE-02-BLG-91	130 ± 123	G7III	0.46 ± 0.20
MACHO-96-BLG-4	112 ± 8	G6III	0.75 ± 0.01
OGLE-02-BLG-69	8 ± 19	G6III	0.78 ± 0.02
MACHO-98-BLG-14	22 ± 16	K2III	1.20 ± 0.01
MACHO-104-C	–10 ± 32	G6III	0.73 ± 0.02
OGLE-00-BUL-43	–15 ± 39	K2III	1.1 ± 0.03
OGLE-02-BLG-100	–36 ± 32	G7V	0.16 ± 0.01
OGLE-02-BLG-61	–123 ± 55	G7III	0.96 ± 0.12
OGLE-99-BLG-19	17 ± 49	K3III	0.79 ± 0.03
sc26_2218	–65 ± 31	G0III	0.68 ± 0.01
sc33_4505	–125 ± 37	K4V	0.50 ± 0.16
OGLE-03-BLG-47	17 ± 33	G5III	0.24 ± 0.15

This method has advantages for low-resolution spectra because the fit is made over all the spectrum, including lines and continuum. More weight is placed on the lines, and in this way, the effect of a single line is not too strong in the classification.

The templates used come from the Jacoby-Hunter-Cristian Atlas list (Jacoby et al. 1984) and the best fit results are summarized in Table 3.

3.3. Results

Results of the best fitting velocity and spectral type in some cases can be compared with older measurements and used to check our procedures.

MACHO-99-BLG-1 and MACHO-98-BLG-6 were classified by Cavallo et al. (2002) as G2V and G8IV respectively, in agreement with our measurements. The reddening results have been tested as well. Event OGLE-99-BLG-19 has $E(V-I) \approx 1.44$ (Smith et al. 2002). This value corresponds to $E(B-V) \approx 0.9$ (using the extinction ratios by Rieke & Lebofsky 1985), which is very close to our determination (see Table 3). This last case is very similar to the event sc26_2218 for which Smith et al. (2003) report a reddening of $E(B-V) \approx 0.56$. Given the large extinction towards the bulge, this value is slightly different to our determination (≈0.1).

Figure 1 shows the velocity histogram for the results in Table 3. A similar histogram has been included in the same figure for a sample of non-microlensed sources selected from the same fields. Particular selection criterion (e.g. *S/N*, proximity to the source, etc.) has not been applied to the non-microlensed sources. However, some disk contamination is expected. Both histograms have been compared by using a Kolmogorov-Smirnov test, which did not allow us to be conclusive about the similarity of both samples.

In the case of reddening we have obtained the histogram in Fig. 2. An agreement is found with the KN03 sample in this parameter, where both samples have the same average reddening. The respective template spectra fits as reported in Table 3 are shown in Fig. 3, where the solid lines are the real spectra and dashed lines correspond to the templates giving the smallest χ^2 in each case.

In general, we have observed a biased spectral classification towards giant G and K stars. This kind of population corresponds to observable bulge stars lying in fields with high foreground dust extinction. At the same time our sample does not show

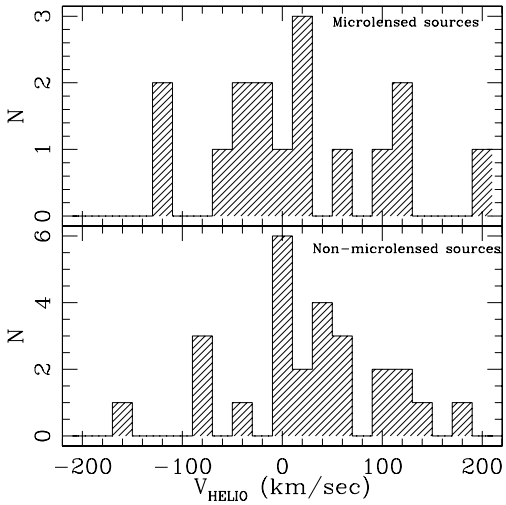

Fig. 1. *Top*: velocity histogram for the microlensing sources. *Bottom*: same as before, but this time for non-microlensed stars in the same fields of the events.

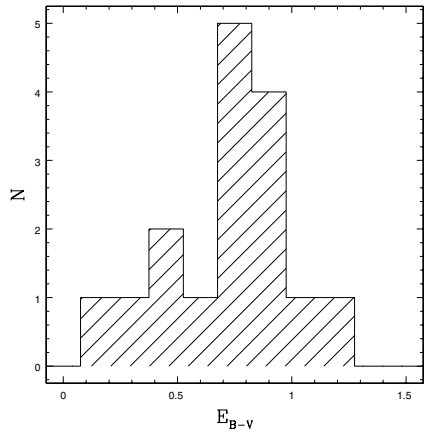

Fig. 2. Extinction distribution for all the microlensing events.

possible candidates where the source is located in the SgrI dwarf galaxy, which has a systematic radial velocity difference relative to bulge members round to ∼200 km s^{-1}, and whose stars are located behind the galactic bulge.

4. Analysis of light curves

4.1. Model

In this section we use two models to fit the microlensing light curves: the standard and the parallax model. This information, combined with the spectroscopic result of the sources, will give a more complete view of the microlensing events.

The standard model of microlensing is able to explain most of the events. This model refers to the situation when velocities are constant for all the objects in the event. This is described with two equations (Paczyński 1986):

$$A(t) = \frac{u^2+2}{u\sqrt{u^2+4}}, \qquad u(t) = \sqrt{u_0^2 + \left(\frac{t-t_0}{\widehat{t}/2}\right)^2}, \tag{1}$$

where $\widehat{t}$ is the time-scale and u_0 is the minimum angular separation between the source and the lens. However, these equations are degenerate, and by including the parallax effect for the longest time scale events (Alcock et al. 1995) we are able to

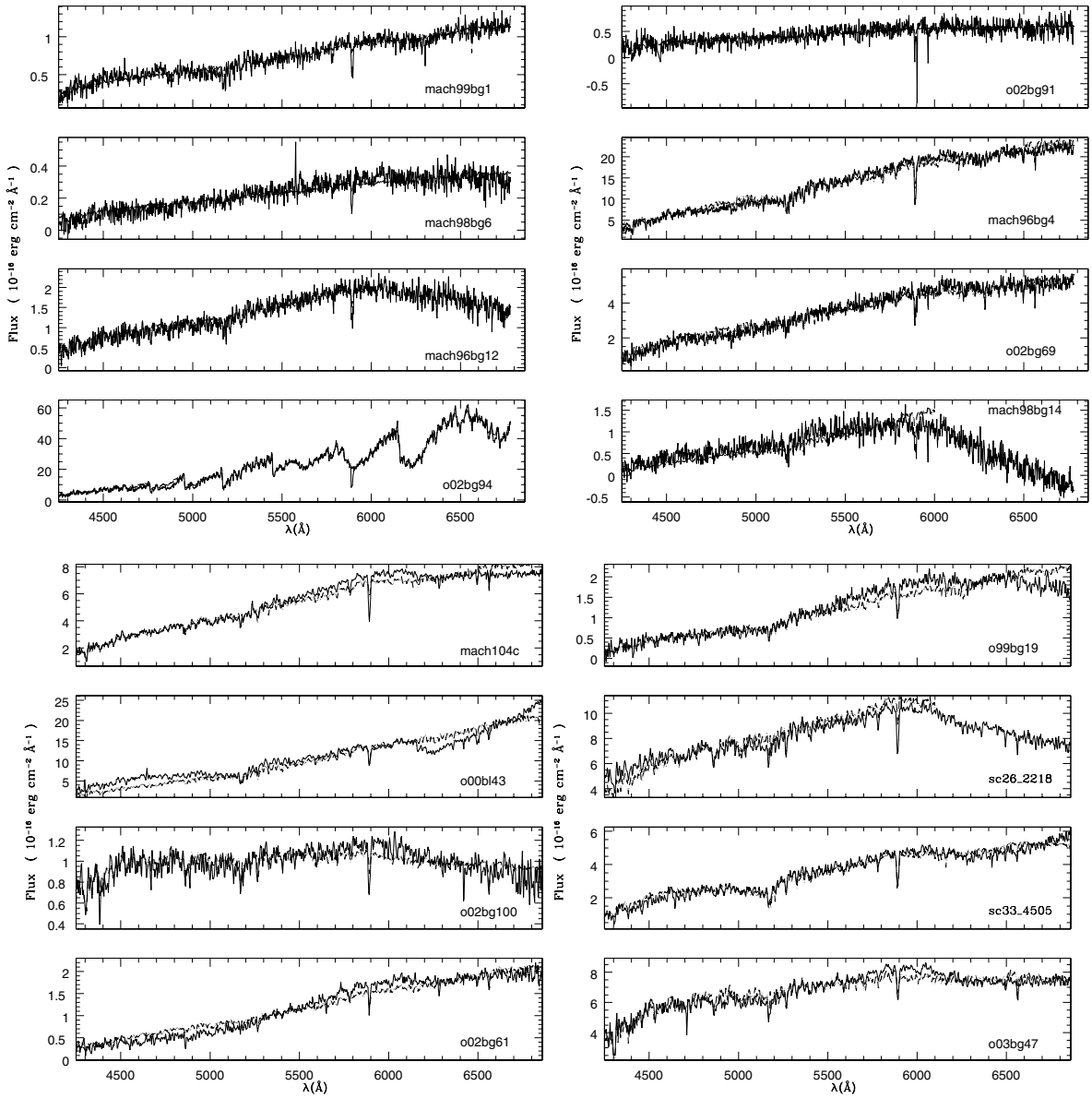

Fig. 3. Spectra (solid) and best fitting models (dashed) obtained using the method of Kane & Sahu for the sources of our microlensing events.

acquire some knowledge about the lens. The parallax influence appears in the equations as

$$\begin{aligned} u^2(t) \;=\; & u_0^2 + \omega^2(t-t_0)^2 + \alpha^2 \sin^2[\Omega(t-t_c)] \\ & +2\alpha \sin[\Omega(t-t_c)][\omega(t-t_0)\sin\theta + u_0\cos\theta] \\ & +\alpha^2 \sin^2\beta\cos^2[\Omega(t-t_c)] \\ & +2\alpha \sin\beta\cos[\Omega(t-t_c)][\omega(t-t_0)\cos\theta - u_0\sin\theta], \end{aligned} \quad (2)$$

where λ and β are the ecliptic latitude and longitude, respectively. θ is the angle between the north axis on the ecliptic and $v_\perp$, $\omega = 2/\widehat{t}$, and t_c is the Earth closest approximation to the line of sight. Therefore, the parameters Ω and α are given by

$$\Omega(t-t_c) = \Omega_0(t-t_c) + 2\varepsilon \sin[\Omega_0(t-t_p)], \quad (3)$$

$$\alpha = \frac{\omega(1\ \mathrm{AU})}{\widetilde{v}} 1 - \varepsilon\cos[\Omega_0(t-t_p)]. \quad (4)$$

where $\Omega_0 = 2\pi\ \mathrm{yr}^{-1}$, the eccentricity is $\epsilon = 0.017$ and t_p is the time of perihelion. The lens mass can be related to the distance of the event and the transversal velocity by

$$M(x) = \frac{(1-x)}{x}\frac{\widetilde{v}^2\widehat{t}^2c^2}{16GD_{ol}}, \quad (5)$$

where $x = D_l/D_s$, D_{ol} is the observer-lens distance and $\widetilde{v}$ is the transversal velocity defined by

$$\widetilde{v} = \frac{v_\perp D_s}{(D_s - D_l)}. \quad (6)$$

We need to add two more parameters to properly describe the data. First, we need to describe the presence of possible blended stars in the light curve. A blending parameter f is usually involved in the expression

$$A_{obs} = Af + 1 - f, \quad (7)$$

where A_{obs} is the observed amplification and the blending parameter will be 1 for a single star without blending. The second parameter I_s is referred to the base level of the amplification light curve, which in our case was made in magnitudes (it

Table 4. Best fitting parameters for the parallax model: t_0 corresponds to the time in the maximum of amplification, $\hat{t}$ is the MACHO timescale, u_0 is related with the maximum approximation to the observer-source line, I_s is the base magnitude of the amplification feature, f the blending parameter (Eq. (7)), $\widetilde{v}$ the transversal velocity and θ is the angle between the transversal velocity and the north axis of the ecliptic, χ^2 corresponds to the best fit for the parallax model, and $\Delta\chi^2$ is the difference between the best standard and parallax fit.

Event	t_0 (days)	$\hat{t}$ (days)	u_0	I_s (mag)	f	$\widetilde{v}$ (Km s^{-1})	θ (rad)	χ^2 $\Delta\chi^2$
M-99-BLG-1	2709.7 ± 2.09	218.43 ± 15.49	0.31 ± 0.02	19.32 ± 0.00	1.00 ± 0.72	37.21 ± 1.37	–1.76 ± 0.48	447 402
M-98-BLG-6	2386.8 ± 4.11	462.53 ± 56.02	0.21 ± 0.05	20.05 ± 0.01	0.71 ± 0.16	80.11 ± 10.35	–1.84 ± 0.28	1232 117
M-96-BLG-12	1742.0 ± 2.54	320.91 ± 32.44	-0.09 ± 0.02	18.30 ± 0.00	0.76 ± 0.16	49.78 ± 3.17	–1.41 ± 0.14	7334 5373
O-02-BLG-94	2409.4 ± 0.02	12.26 ± 0.02	3.10 ± 0.00	14.08 ± 0.00	0.94 ± 0.00	55.86 ± 0.072	–0.47 ± 0.00	1163 7
O-02-BLG-91	2454.9 ± 0.45	487.26 ± 15.46	0.08 ± 0.00	18.52 ± 0.00	0.01 ± 0.00	20.71 ± 0.16	–1.29 ± 0.01	145 9
M-96-BLG-4	1535.9 ± 1.29	118.62 ± 1.62	0.13 ± 0.05	16.771 ± 0.00	1.00 ± 0.06	67.09 ± 7.90	–3.15 ± 0.05	1251 48
	2139.1 ± 2.36	124.38 ± 1.87	0.95 ± 0.04	16.769 ± 0.00	1.00 ± 0.89	42.07 ± 5.10	–3.08 ± 0.03	1083 28
O-02-BLG-69	2444.1 ± 0.11	139.89 ± 1.60	0.11 ± 0.00	16.15 ± 0.00	1.00 ± 0.00	28.27 ± 0.17	–2.33 ± 0.01	363 075 3987
M-98-BLG-14	2363.4 ± 0.85	49.52 ± 6.35	0.72 ± 0.11	18.26 ± 0.00	0.20 ± 0.05	22.66 ± 0.19	–1.28 ± 0.03	332 92
M-104-C	506.23 ± 0.48	248.40 ± 2.68	0.11 ± 0.01	17.81 ± 0.00	0.77 ± 0.01	81.64 ± 3.01	–1.39 ± 0.110	5866 7904
O-00-BUL-43	1865.2 ± 0.53	326.00 ± 9.60	0.18 ± 0.01	13.76 ± 0.00	0.87 ± 0.053	40.73 ± 1.50	–2.35 ± 0.024	3115 4218
O-02-BLG-100	2444.6 ± 0.06	46.58 ± 1.41	0.41 ± 0.02	17.87 ± 0.00	0.27 ± 0.01	34.88 ± 0.56	–1.33 ± 0.01	220 921
O-02-BLG-61	2501.4 ± 0.50	358.74 ± 17.61	0.08 ± 0.02	17.35 ± 0.01	0.65 ± 0.04	94.12 ± 17.66	–0.77 ± 0.11	458 450
O-99-BLG-19	1668.4 ± 1.14	751.22 ± 8.06	-0.48 ± 0.01	16.05 ± 0.00	0.78 ± 0.13	12.356 ± 0.09	–2.92 ± 0.01	743 18 311
O-03-BLG-47	2843.7 ± 5.62	332.30 ± 59.08	0.66 ± 0.19	16.09 ± 0.00	0.50 ± 0.23	105.47 ± 23.68	–2.83 ± 0.14	155 69

can be defined in terms of relative amplification as well, since $I_{obs} = I_s + -2.5\ \log(A_{obs})$). Therefore the free parameters in every case are five (u_0, t_0, $\widehat{t}$, I_s, f), and seven (u_0, t_0, $\widehat{t}$, I_s, f, $\widetilde{v}$, θ) for standard and parallax models respectively.

The standard and parallax fits were performed using MINUIT[1] from the CERN library. The results for the best parallax fits are given in Table 4, where $\Delta\chi^2$ is the difference between the best χ^2 between the standard and parallax models; this is a good indicator of the deviation effect produced by parallax.

Events *sc26_2218* and *sc33_4505* were excluded from this analysis because they do not have data on the same scale as MACHO or OGLE. In particular for event *sc26_2218* Smith et al. (2003) performed a mass determination, which suggested a brown dwarf lens ($M_{lens} \sim 0.05\ M_\odot$).

4.2. Description of derived light curves

The parallax represents the influence of the change in the Earth position during the event. This influence will be stronger if the time scale is longer. Typically, a long time scale is associated with a transversal velocity that is not too large.

We have found three events with a weak parallax signal, the events OGLE-02-BLG-94, OGLE-02-BLG-91 and MACHO-96-BLG-4, where the third of these events corresponds to a binary event. Binary events are produced when one of the components of the microlensing effect (source or lens) is binary. The presence of a second mass as a lens or source produces changes in the light curve that in most cases requires changes in the respective fit.

During the analysis of MACHO-96-BLG-4 (which was previously analyzed by Alcock et al. 2000b) we decided to use the simple parallax model and not a binary model. This is compatible with the data considering that there is no caustic in the amplification light curve used and between the two maxima the baseline level is reached; both maxima are separated by more than 500 days. These arguments suggest that the system in this case should not be a tight binary. Consequently, the fit was carried out for each maximum keeping the same baseline magnitude (I_s), where the results correspond to two sets of parameters; these results do not allow us to discriminate between a lens or source binary. Nevertheless, our spectrum for MACHO-96-BLG-4 does not show double or wide lines, which characterize a binary source. Furthermore, the cross correlation during the velocity measurement has a single well defined peak, and therefore, the velocity has a small uncertainty in this case, favoring a binary lens. We obtain for the difference in transversal velocities and t_0 a separation of 8.7 AU; likewise by Eq. (5) a mass ratio of $q = M_2/M_1 \approx 0.43$ can be obtained. Note that the last value has assumed equal distances for both maxima, which is not considered in Sect. 5, where the likelihood function delivers different distance estimations for the event and therefore a different mass ratio M_2/M_1.

The second event with a binary signature is OGLE-02-BLG-69 (Cassan et al. 2004). This is clear only from the shape of the

[1] Available in `http://wwwinfo.cern.ch/asd/cernlib/`.

light curve, yielding the largest χ^2 in the sample (Table 4). Again we do not observe spectral features indicative of a binary source, therefore we favor the binary lens option for this event as well. The right way to find the parameters in this case should be with a binary lens model which is beyond of the scope of this paper; the parallax model is insufficient.

The best illustration of the difference between the standard and parallax model corresponds to the event OGLE-99-BLG-19 (Smith et al. 2002). This event has several special properties such as secondary peaks (it is known as a "*mutiparallax* event"), a very long time-scale (almost as long as MACHO99-BLG-32/OGLE-99-BLG-32, the longest time scale registered) and a very small transversal velocity. All these peculiarities will be discussed in Sect. 5.

The events MACHO-99-BLG-1, MACHO-98-BLG-6, MACHO-96-BLG-12 and OGLE-00-BUL-43 were useful as a proof for the method. The first three events were analyzed by Bennett et al. (2002), and the last one was analyzed by Soszyński et al. (2001), with very similar results to ours in the four cases.

Three events from our list have never been analyzed before, OGLE-02-BLG-61, OGLE-02-BLG-100 and OGLE-03-BLG-47. They have $\Delta\chi^2$ that indicates a significant parallax. Figure 4 shows the best set of parameters for these three events from fits performed with MINUIT.

It is commonly assumed that distances within the event are known, or at least constrained. Along the line of sight toward the bulge the sources can lie in three places: disk, bulge, or in the dSph Sagittarius galaxy behind the bulge. The velocity distribution in each place is different. While the disk has a flat rotation at approximately 220 km s^{-1} with a dispersion close to 30 km s^{-1}, the bulge has a small rotation with a dispersion of 80–100 km s^{-1} (Minniti 1996), and Sagittarius is moving away from the Sun at 150 km s^{-1} (Ibata et al. 1997). Therefore a preliminary classification can be made in some spectra according to the velocity values obtained. For instance in OGLE-00-BUL-43 we find an unusually low transversal and radial velocity, with values more likely for disk events. A similar situation is found for events OGLE-02-BLG-100, MACHO-98-BLG-14 and OGLE-99-BLG-19. Although OGLE-02-BLG-69 also has low velocities, the distance determination of this event is uncertain because it is a binary event. However, we have four events consistent with disk velocities.

Distant events located behind the bulge should have higher extinction than closer events. This is based on the fact that self-lensing inside the bulge has a larger Einstein ring when the distance between the lens and the source is larger, and therefore the extinction for the events within the bulge should increase when the timescale increases. We have eliminated disk events on the plot of extinction vs. timescale (Fig. 5) to prove this hypothesis and compare with a equivalent plot for the KN03 sample. For our events we have obtained a tiny negative slope of −0.0003, which is not significant enough if we compare it with KN03 (0.018). This disagreement can be explained by the original selection of special events which included events with unusual properties (e.g. MACHO-98-BLG-6).

In our sample we identified some events with sources lying in the bulge, while no sources in Sagittarius were identified. Sagittarius events are very important because their identification would mean a change in the determination for the bulge optical depth τ (Cserenjes & Alard 2001) and therefore the angle assumed for the bar inside the galactic bulge. Sagittarius events with detectable parallax have 20 times greater probability of being observed (Bennett et al. 2002) than bulge events with

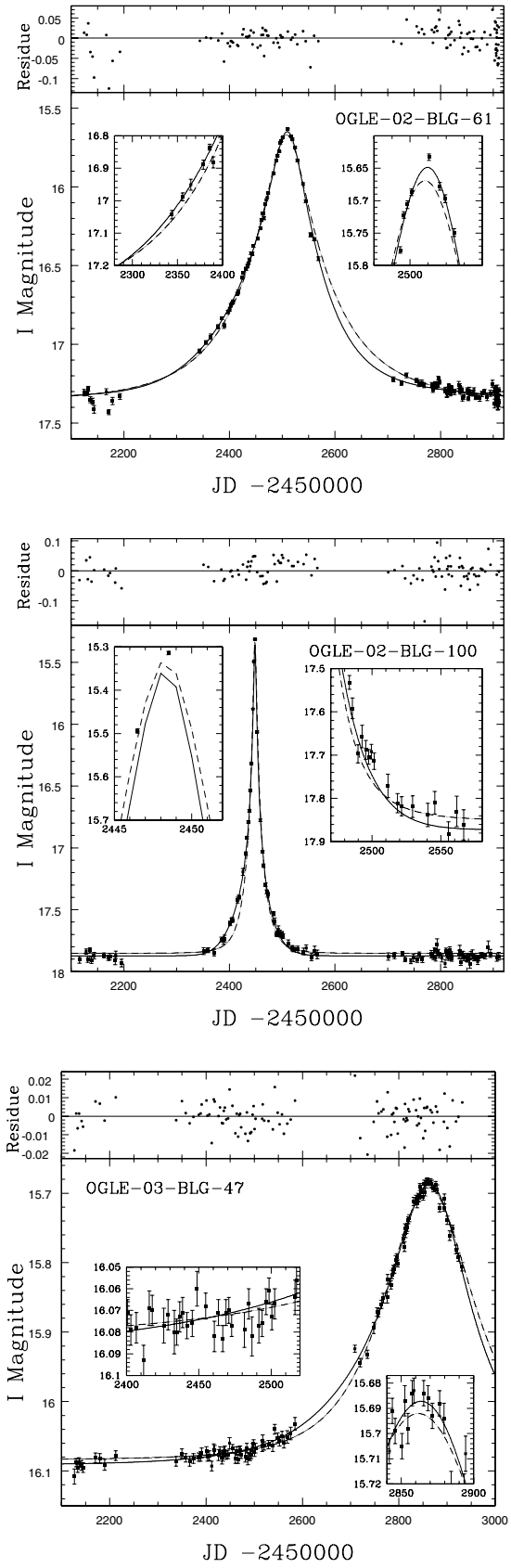

Fig. 4. Example of the results obtained with MINUIT fit in the amplification light curve for the three events not analyzed before: OGLE-02-BLG-61 (*top*), OGLE-02-BLG-100 (*middle*) and OGLE-03-BLG-47 (*bottom*).

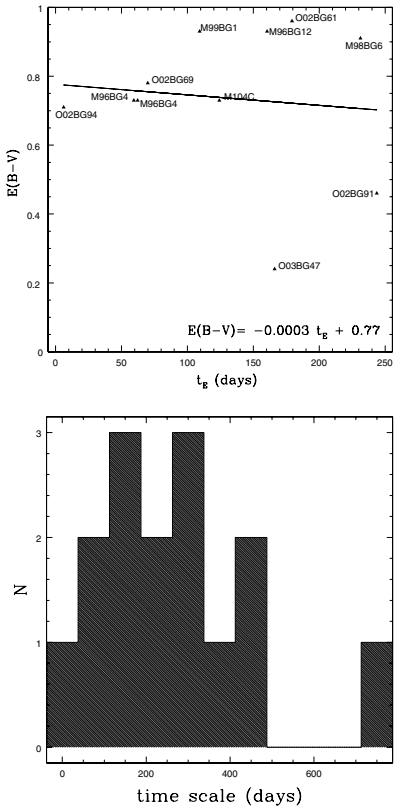

Fig. 5. *Top*: extinction versus the timescale excluding disk events. We have rejected disk events and the binary events to compare with previous works. *Bottom*: distribution of timescale in the whole sample, including disk events.

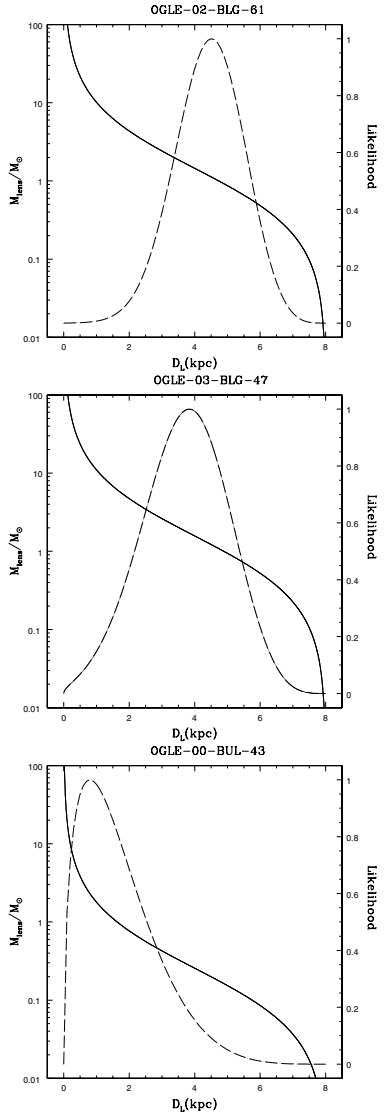

Fig. 6. Examples of mass estimations for three events of the sample. The solid line corresponds to the mass estimation according to the values found for the best microlensing light curve fit in each case. The mass values are constrained combining the mass function with a likelihood curve (dashed line) given by a galaxy model. The maximum likelihood in the mass function are presented in Table 5. While the third event OGLE-00-BLG-43 shows the maximum likelihood for a lens in the solar neighborhood, the first two objects show the presence of their lenses in the disk region close to the limits of the bulge.

detectable parallax. The fact that most of the events detected are produced in the bulge is because stars in the bulge are more numerous. The search for Sagittarius events could give us results that could change our understanding of the morphology of our Galactic center. The high foreground extinction in fields close the galactic plane makes very difficult observations towards the galactic bulge, and is the reason why the bar signature is better constrained by gas models than stars.

5. Mass determinations

The lens mass according to Eq. (5) depends on the relative distances, the timescale, and transversal velocity. We can estimate the lens mass using a likelihood function (Alcock et al. 1995) as follows

$$L(x;\widetilde{v}) \propto \sqrt{x(1-x)}\rho_{\rm L}(x)\widetilde{v}(1-x)^3 \times \int f_{\rm s}(\boldsymbol{v}_{\rm s}) f_{\rm l}((1-x)(\boldsymbol{v}_\odot + \widetilde{\boldsymbol{v}}) + x\boldsymbol{v}_{\rm s}) {\rm d}\boldsymbol{v}_{\rm s}, \quad (8)$$

where $\rho_{\rm L}$ (Han & Gould 1995; Belokurov & Evans 2002) corresponds to the density of lenses at distance $x = D_{\rm l}/D_{\rm s}$, and $f_{\rm s}$ and $f_{\rm l}$ are the source and lens velocity distributions (Han & Gould 1996). The integral is over combinations of source and lens velocities ($\boldsymbol{v}_{\rm s}$ and $\boldsymbol{v}_l = (1-x)(\boldsymbol{v}_\odot + \widetilde{\boldsymbol{v}}) + x\boldsymbol{v}_{\rm s}$ respectively) in two dimensions. We have assumed a disk velocity dispersion of 30 km s^{-1} in each direction with a flat rotation of 220 km s^{-1}. The dispersions inside the bulge were taken from Han & Gould (1996) considering no bulge rotation. The resulting likelihood function is shown as a dashed line in Fig. 6 for some events. In Table 5 we list the "most likely" parameters. To obtain these results we had to assume in each case the location of the source. This was made according the radial and transversal velocities measured in the previous steps and the known velocity distribution in the disk and bulge. We assumed bulge sources at 8 kpc and disk sources at 4 kpc respectively. The resulting masses in some cases are large enough to suggest black holes; the small blending parameter favours this possibility. The best candidates are MACHO-98-BLG-6 (reported by Bennett et al. 2002) and OGLE-00-BUL-43 (reported by Soszyński et al. 2001). For the case of MACHO-98-BLG-6 the source was assumed to be in the bulge at 8 kpc, in the case of OGLE-00-BUL-43 the source was set in the disk. The reason for a source inside the disk was the low transversal velocity, more likely for a disk-disk event. The case for the source lying in the bulge was made for

Table 5. Most likely parameters according to lens likelihood function.

Event	$D_{\rm lens}$ (kpc)	$M/M_\odot$	source location
MACHO-99-BLG-1	0.9	$0.6^{+1.0}_{-0.5}$	bulge
MACHO-98-BLG-6	1.9	6^{+9}_{-4}	bulge
MACHO-96-BLG-12	1.6	$1.3^{+1.5}_{-0.8}$	bulge
OGLE-02-BLG-94	3.2	$0.001^{+0.001}_{-0.0006}$	bulge
OGLE-02-BLG-91	1.1	$0.8^{+1.3}_{-0.6}$	bulge
MACHO-96-BLG-4	2.4	$0.2^{+0.3}_{-0.1}$	bulge
	1.2	$0.2^{+0.5}_{-0.1}$	bulge
OGLE-02-BLG-69	...	...	...
MACHO-98-BLG-14	0.6	$0.020^{+0.05}_{-0.015}$	disk
MACHO-104-C	3.4	$0.73^{+0.67}_{-0.43}$	bulge
OGLE-00-BUL-43	0.5	$2.9^{+6.1}_{-1.9}$	disk
OGLE-00-BUL-43	0.8	$2^{+6}_{-1.5}$	bulge
OGLE-02-BLG-100	0.8	$0.03^{-0.01}_{+0.06}$	disk
OGLE-02-BLG-61	4.5	$1.1^{+0.9}_{-0.6}$	bulge
OGLE-99-BLG-19	0.5	$1.6^{+2.1}_{-1.0}$	disk
OGLE-03-BLG-47	3.8	$1.7^{+1.6}_{-1.0}$	bulge

OGLE-00-BUL-43 as well; the initial mass dropped from 2.86 to 2.06 $M_\odot$, where this lens mass might still be a black hole. A mass inside this range should correspond to a main sequence A5-A0 star which did not appear in the images.

The situation of a disk-disk event is even clearer for OGLE-99-BLG-19, where the velocities lie between the limits for the disk. The "most likely distance" in this case was 0.5 kpc, therefore, the corresponding spectral type for the lens is a F0V star. Even though two more events have been identified with lenses and sources lying in the disk, MACHO-98-BLG-14 and OGLE-02-BLG-100, their mass estimations are not reliable due to their short timescales ($\hat{t}$) and therefore weak parallax.

This analysis has not been applied to OGLE-02-BLG-69. As we have explained before this event requires a binary model, which is beyond the scope of this paper.

6. Summary and conclusions

We have presented spectra for 16 microlensed sources and the amplification light curve analysis for 14 of them. The spectra were taken with the Magellan telescopes I and II, and the photometry of the light curves comes from the public data from MACHO and OGLE pages.

We have used the spectra to obtain radial velocities, spectral types and extinction. Extinction spanned a broad range in agreement with the known uneven foreground extinction in the galactic bulge and distances estimated using the likelihood function. In general, larger extinction correspond to longer timescales; in our case this behavior has not been observed. However, this is a small sample of unusual events, which may have biased our results.

Radial velocities in the sample show values in agreement with bulge membership in most of the cases. We have shown that two events are due to a disk-disk configuration, OGLE-99-BLG-19 and OGLE-00-BUL-43, with a strong parallax signature and low radial and transversal velocities.

Most of the events analyzed here have a strong parallax. We have also analyzed three events with weak parallax effects. The results on OGLE-02-BLG-94, OGLE-02-BLG-91 and OGLE-02-BLG-100 do not show a strong difference between the fit with the standard and the parallax model.

The likelihood function to determine the "most likely" lens parameters based on the results of the parallax fit shows in two cases events with large lens masses, MACHO-98-BLG-6 and OGLE-00-BUL-43. According to these masses they should correspond to bright stars for which we have not found evidence. They can be considered therefore as black hole candidates. However, the large uncertainties in these masses must be considered.

Acknowledgements. We thank the anonymous referee for a number of suggestions that considerably improved the quality of this manuscript. We acknowledge the kind hospitality and efficiency of the staff at Las Campanas Observatory. D.M. is supported by FONDAP Center for Astrophysics 15010003, and by a Fellowship from the John Simon Guggenheim Foundation.

References

Alcock, C., Allsman, R. A., Alves, D., et al. 1995, ApJ, 454, L125
Alcock, C., Allsman, R. A., Alves, D. R., et al. 1999, PASP, 111, 1539A
Alcock, C., Allsman, R. A., Alves, D. R., et al. 2000a, ApJ, 542, 281
Alcock, C., Allsman, R. A., Alves, D., et al. 2000b, ApJ, 541, 270
Beaulieu, J.-P., Bennett, D. P., Fouqué, P., et al. 2006, Nature, 439, 437
Belokurov, V., & Evans, N. W. 2002, MNRAS, 331, 649
Bennett, D., Becker, A. C., Quinn, J. L., et al. 2002, ApJ, 579, 639
Binney, J., Gerhard, O. E., Stark, A. A., Bally, J., & Uchida, K. I. 1991, MNRAS, 252, 210
Bond, I. A., Udalski, A., Jaroszynski, M., et al. 2004, ApJ, 606, L155
Cassan, A., Beaulieu, J. P., Brillant, S., et al. 2004, A&A, 419, L1
Cavallo, R. M., Cook, K. H., Minniti, D., & Vandehei, T. 2003, SPIE, 4834, 66
Cserenjes, P., & Alard, C. 2001, A&A, 369, 778
Han, C., & Gould, A. 1995, ApJ, 447, 53
Han, C., & Gould, A. 1996, ApJ, 467, 540
Han, C., & Gould, A. 1997, ApJ, 480, 196
Han, C., & Gould, A. 2003, ApJ, 592, 172
Ibata, R. A., Wyse, R. F., Gilmore, G., Irwin, M. J., & Suntzeff, N. B. 1997, AJ, 113, 634
Jacoby, G. H., Hunter, D. A., & Christian, C. A. 1984, ApJS, 56, 257
Kane, S. R., & Sahu, K. C. 2003, ApJ, 582, 743
Kane, S. R., & Sahu, K. C. 2006, ApJ, 637, 752
Minniti, D. 1996, ApJ, 459, 175
Paczyński, B. 1986, ApJ, 304, 1
Popowski, P., Griest, K., Thomas, C. L., et al. 2005, ApJ, 631, 879
Rieke, G. H., & Lebofsky, M. J. 1985, ApJ, 288, 618
Seaton, M. J. 1979, MNRAS, 187, 73
Smith, M. C., Mao, S., & Woźniak, P. 2002, MNRAS, 336, 670
Smith, M. C., Mao, S., & Woźniak, P. 2003, ApJ, 585, L65
Soszyński, I., Zebrun, K., Wozniak, P. R., et al. 2001, ApJ, 552, 731
Sumi, T., Wozniak, P. R., Udalski, A., et al. 2006, ApJ, 636, 240
Tonry, J., & Davis, M. 1979, AJ, 84
Udalski, A., Jaroszynski, M., Paczynski, B., et al. 2005, ApJ, 628, L109
Wood, A., & Mao, S. 2005, MNRAS, 362, 945
Wózniak, P. R., Udalski, A., Szymański, M., et al. 2001, AcA, 51, 175